Chemical Engineering Journal 281 (2015) 813–825

Contents lists available at ScienceDirect

Chemical Engineering Journal

journal homepage: www.elsevier.com/locate/cej

# Real gas transport through nanopores of varying cross-section type and shape in shale gas reservoirs

Keliu Wu [a,b,*], Zhangxin Chen [a], Xiangfang Li [b]

[a] Chemical and Petroleum Engineering, University of Calgary, Alberta T2N1N4, Canada
[b] Key Laboratory for Petroleum Engineering of the Ministry of Education, China University of Petroleum, Beijing 102249, China

## HIGHLIGHTS

- A model for real gas transport through nanopores of shale gas reservoirs was proposed.
- Gas transport behavior in nanopores of shale gas reservoirs was revealed.
- Nanopore type, shape and size significantly influence gas transport.
- Real gas effect enhances gas transport capacity in nanopores.

## ARTICLE INFO

*Article history:*
Received 18 April 2015
Received in revised form 29 June 2015
Accepted 3 July 2015
Available online 9 July 2015

*Keywords:*
Shale gas reservoirs
Nanopores
Real gas
Slip flow
Knudsen diffusion

## ABSTRACT

A model for real gas transport in nanopores of shale gas reservoirs (SGRs) was proposed on the basis of the weighted superposition of slip flow and Knudsen diffusion, where the ratios of the intermolecular collisions and the molecule–nanopore wall collisions to the total collisions are the weighted factors of slip flow and Knudsen diffusion, respectively. The present model takes account of slip effect and real gas effect, additionally, the effects of cross-section type and its shape of nanopores on gas transport are also considered in this paper. The present model is successfully validated against existing molecular simulation data collected from different sources in literature. The results show: (1) the present model is reasonable to describe all of the gas transport mechanisms known, including continuum flow, slip flow and transition flow in nanopores of SGRs; (2) the cross-section type and shape of nanopores both affect gas transport capacity: at the same cross-sectional area, gas transport capacity of nanopores with a circular cross section is greater than that with a rectangular cross section, and gas transport capacity of nanopores with a rectangular cross section decreases with an increasing aspect ratio; compared to the cross-section type, the effect of the cross-section shape on gas transport capacity is stronger; (3) a real gas effect improves gas transport capacity, which becomes more obvious with an increasing pressure and a decreasing pore size; (4) and compared to nanopores with a circular cross section, the effect of real gas effect on gas transport capacity of nanopores with a rectangular cross section is stronger, and the effect increases with an increasing aspect ratio. The proposed model can provide some theoretical support in numerical simulation of reservoir behavior in SGRs.



## 1. Introduction

Currently, gas transport in nanopores have been the focus of a large number of studies [1–6]. Due to the improved horizontal-drilling and hydraulic-fracturing technologies, the commercial gas production of SGRs with a large reserve is being achieved in North America, which has received a great of attention around the world [7]. Shale gas transport in nanopores is the basis for accurate numerical simulation, which provides theoretical and technical support for gas production prediction and fracture parameter optimization in SGRs [8].

Nanopores are abundant in SGRs, and their diameters range from a few nanometers to several hundred nanometers [9], which causes that gas transport in SGRs is significantly different from that in conventional gas reservoirs [10,11]. Based on Knudsen number $K_n$, defined as the ratio of gas mean free path to the characteristic dimension, gas transport mechanisms are classified into continuum flow ($K_n < 10^{-3}$), slip flow ($10^{-3} < K_n < 10^{-1}$) and transition flow ($10^{-1} < K_n < 10$) in nanopores of SGRs [8]. The Navier–Stokes equation is only valid for continuum flow [12]; for slip flow,

* Corresponding author at: Chemical and Petroleum Engineering, University of Calgary, Alberta T2N1N4, Canada. Tel.: +1 (403) 966 3673.
*E-mail address:* wukeliu19850109@163.com (K. Wu).

http://dx.doi.org/10.1016/j.cej.2015.07.012
1385-8947/

**Nomenclature**

| | |
|---|---|
| $A(\zeta)$ | section shape factor of nanopores with a rectangular cross section for slip flow, dimensionless |
| $A_1$ | fitting constant, dimensionless |
| $A_2$ | fitting constant, dimensionless |
| $A_3$ | fitting constant, dimensionless |
| $B(\zeta)$ | section shape factor of nanopores with a rectangular cross section for Knudsen diffusion, dimensionless |
| $b$ | gas slip constant, dimensionless |
| $C_{\text{app-tr}}$ | the apparent gas conductance of shale matrix, s |
| $C_{\text{C-ki}}$ | ideal gas conductance of Knudsen diffusion through nanopores with a circular cross section, s |
| $C_{\text{C-kr}}$ | real gas conductance of Knudsen diffusion through nanopores with a circular cross section, s |
| $C_{\text{C-ti}}$ | total conductance for ideal gas through nanopores with a circular cross section, s |
| $C_{\text{C-tr}}$ | total conductance for real gas through nanopores with a circular cross section, s |
| $C_{\text{C-vsi}}$ | ideal gas conductance of slip flow through nanopores with a circular cross section, s |
| $C_{\text{C-vsr}}$ | real gas conductance of slip flow through nanopores with a circular cross section, s |
| $C_{\text{g}}$ | gas compressibility, 1/MPa |
| $C_{\text{R-ki}}$ | ideal gas conductance of Knudsen diffusion through nanopores with a rectangular cross section, s |
| $C_{\text{R-kr}}$ | real gas conductance of Knudsen diffusion through nanopores with a rectangular cross section, s |
| $C_{\text{R-ti}}$ | total conductance for ideal gas through nanopores with a rectangular cross section, s |
| $C_{\text{R-tr}}$ | total conductance for real gas through nanopores with a rectangular cross section, s |
| $C_{\text{R-vsi}}$ | ideal gas conductance of slip flow through nanopores with a rectangular cross section, s |
| $C_{\text{R-vsr}}$ | real gas conductance of slip flow through nanopores with a rectangular cross section, s |
| $D_{\text{f}}$ | fractal dimension of the pore wall, dimensionless |
| $h$ | height of a rectangular cross section for nanopores, m |
| $J_{\text{C-ki}}$ | Knudsen diffusion mass flux for ideal gas through nanopores with a circular cross section, kg/(m$^2$ s) |
| $J_{\text{C-kr}}$ | Knudsen diffusion mass flux for real gas through nanopores with a circular cross section, kg/(m$^2$ s) |
| $J_{\text{C-ti}}$ | total mass flux for ideal gas through nanopores with a circular cross section, kg/(m$^2$ s) |
| $J_{\text{C-ti}}/J_{\text{C-ki}}$ | dimensionless ideal gas flux based on Knudsen diffusion flux through nanopores with a circular cross section, dimensionless |
| $J_{\text{C-ti}}/J_{\text{C-vi}}$ | dimensionless ideal gas flux based on continuum flow flux through nanopores with a circular cross section, dimensionless |
| $J_{\text{C-tr}}$ | total mass flux of real gas through nanopores with a circular cross section, kg/(m$^2$ s) |
| $J_{\text{C-vi}}$ | continuum flow mass flux for ideal gas through nanopores with a circular cross section, kg/(m$^2$ s) |
| $J_{\text{C-vsi}}$ | slip flow mass flux for ideal gas through nanopores with a circular cross section, kg/(m$^2$ s) |
| $J_{\text{C-vsr}}$ | slip flow mass flux for real gas through nanopores with a circular cross section, kg/(m$^2$ s) |
| $J_{\text{R-ki}}$ | Knudsen diffusion mass flux for ideal gas through nanopores with a rectangular cross section, kg/(m$^2$ s) |
| $J_{\text{R-kr}}$ | Knudsen diffusion mass flux for real gas through nanopores with a rectangular cross section, kg/(m$^2$ s) |
| $J_{\text{R-ti}}$ | total mass flux for ideal gas through nanopores with a rectangular cross section, kg/(m$^2$ s) |
| $J_{\text{R-ti}}/J_{\text{R-ki}}$ | dimensionless ideal gas flux based on Knudsen diffusion flux through nanopores with a rectangular cross section, dimensionless |
| $J_{\text{R-ti}}/J_{\text{R-vi}}$ | dimensionless ideal gas flux based on continuum flow flux through nanopores with a rectangular cross section, dimensionless |
| $J_{\text{R-tr}}$ | total mass flux of real gas through nanopores with a rectangular cross section, kg/(m$^2$ s) |
| $J_{\text{R-vi}}$ | continuum flow mass flux for ideal gas through nanopores with a rectangular cross section, kg/(m$^2$ s) |
| $J_{\text{R-vsi}}$ | slip flow mass flux for ideal gas through nanopores with a rectangular cross section, kg/(m$^2$ s) |
| $J_{\text{R-vsr}}$ | slip flow mass flux for real gas through nanopores with a rectangular cross section, kg/(m$^2$ s) |
| $Kn_{\text{i}}$ | Knudsen number for ideal gas, dimensionless |
| $Kn_{\text{r}}$ | Knudsen number of real gas, dimensionless |
| $l$ | gas transport distance, m |
| $M$ | gas molar weight, kg/mol |
| $p$ | pressure, MPa |
| $p_{\text{c}}$ | critical pressure of gas, MPa |
| $p_{\text{r}}$ | reduced pressure of gas, dimensionless |
| $R$ | universal gas constant, J/(mol k) |
| $r$ | pore radius, m |
| $S$ | cross-sectional area of nanopores, nm$^2$ |
| $T$ | reservoir temperature, K |
| $T_{\text{c}}$ | critical temperature of gas, K |
| $T_{\text{r}}$ | reduced temperature of gas, dimensionless |
| $w$ | width of a rectangular cross section for nanopores, m |
| $Z$ | gas compressibility factor, dimensionless |

*Greek letters*

| | |
|---|---|
| $\phi$ | porosity, decimal |
| $\alpha_{\text{i}}$ | rarefaction coefficient of ideal gas, dimensionless |
| $\alpha_{\text{o}}$ | rarefaction coefficient when $K_{\text{n}} \to \infty$, dimensionless |
| $\alpha_{\text{r}}$ | rarefied coefficient of real gas, dimensionless |
| $\alpha_1$ | fitting constant, dimensionless |
| $\beta$ | fitting constant, dimensionless |
| $\eta$ | gas viscosity at $p = 1.01325 \times 10^5$ Pa and $T = 423$ K, p$_{\text{a}}$ s |
| $\eta_{\text{r}}$ | real gas viscosity, p$_{\text{a}}$ s |
| $\lambda_{\text{i}}$ | mean free path of ideal gas, m |
| $\lambda_{\text{r}}$ | mean free path of real gas, m |
| $\xi$ | aspect ratio of nanopores with a rectangular cross section, dimensionless |
| $\sigma$ | ratio of normalized molecule size to local average pore diameter, dimensionless |
| $\tau$ | tortuosity, dimensionless |
| $\psi$ | deviation degree of gas transport mass between real gas and ideal gas, % |
| $\omega_{\text{C-ki}}$ | weighting coefficient for Knudsen diffusion through nanopores with a circular cross section for ideal gas, dimensionless |
| $\omega_{\text{C-kr}}$ | weighting coefficient for Knudsen diffusion through nanopores with a circular cross section for real gas, dimensionless |
| $\omega_{\text{C-vsi}}$ | weighting coefficient for slip flow through nanopores with a circular cross section for ideal gas, dimensionless |
| $\omega_{\text{C-vsr}}$ | weighting coefficient for slip flow through nanopores with a circular cross section for real gas, dimensionless |
| $\omega_{\text{R-ki}}$ | weighting coefficient for Knudsen diffusion through nanopores with a rectangular cross section for ideal gas, dimensionless |

| | | | |
|---|---|---|---|
| $\omega_{R\text{-}kr}$ | weighting coefficient for Knudsen diffusion through nanopores with a rectangular cross section for real gas, dimensionless | $\omega_{R\text{-}vsr}$ | weighting coefficient for slip flow through nanopores with a rectangular cross section for real gas, dimensionless |
| $\omega_{R\text{-}vsi}$ | weighting coefficient for slip flow through nanopores with a rectangular cross section for ideal gas, dimensionless | | |

Navier–Stokes equations with the corrected slip flow boundary condition, including the first-order and second-order slip flow equations, are valid [13]; for transition flow, compared with experimental results, gas transport calculated by the first-order slip flow equation is underestimated [14]; there are large variations in the second-order slip coefficient for the second-order slip flow equation, and the lack of a universally accepted second-order slip coefficient is a major problem when it is applied to transition flow [13].

As mentioned above, a single constitutive equation can't describe all the gas transport mechanisms known in nanopores of SGRs. Hence, a lot of scholars proposed a variety of unified equations to attempt to overcome this problem [8,15–23]. Unfortunately, these unified equations, based on the superposition of different gas transport mechanisms, are not valid because of different defects, as shown in Table 1. Therefore, a robust model is urgently developed to model gas transport accurately in nanopores of SGRs.

There is a severe thermodynamic nonequilibrium, named as slip effect, in gas transport through nanopores of SGRs, which is a common physic phenomenon also occurring in gas transport for adsorptive gas separation, heterogeneous catalysis, an electrochemical process under a low pressure condition [24–26]. In addition, gas transport in nanopores of SGRs has its particularity due to an extremely high reservoir pressure of 20–60 MPa [27], named the real gas effect, which refers to that the gas intermolecular force and molecules themselves volume both significantly affect gas transport in nanopores [22]. Therefore, the quantitative characterization of real gas effect on gas transport through nanopores of SGRs also need to be resolved.

Nanopores in SGRs are complex with diverse cross-section types and shapes, including triangular, circular, rectangular, and trapezoidal cross sections, as shown in Fig. 1 [28]. The majority of existing gas transport models in SGRs are established with an assumption of nanopores with a circular cross section, and do not consider the differences between gas transport in nanopores with different cross-section types and shapes [8,15–19,22]. However, the existing experiments show that the cross-section type and shape affect gas transport in continuum region [29], a gas mass flux is related to a cross-sectional area, perimeter, and so on, and it can be calculated by correcting the equivalent hydrodynamic radius for nanopores with different cross sections [12,30]. For the slip region and transition region, the strong collision between the gas molecules and the nanopore wall affect the gas transport behavior [31], and nanopores with different cross-section types and shapes have different specific surface. Therefore, the cross-section type and shape also affect gas transport behavior in slip and transition regions [32–35]. Due to the diversity of nanopores in SGRs, finding analytical solutions for


**Fig. 1.** Diversity of nanopores in shale gas reservoirs.

**Table 1**
Comparison and evaluation of different gas transport models in naopores.

| Model | Description | Limitation |
|---|---|---|
| Ertekin et al. (1986) [15] | Weighted superposition based on continuum flow and Fick diffusion | Constant weighted factors; without consideration of real gas effect; only for nanopores with a circular cross-section |
| Liu et al. (2002) [16] | Weighted superposition based on continuum flow and Knudsen diffusion | Invalid for $K_n \geqslant 1$; without consideration of real gas effect; only for nanopores with a circular cross-section |
| Javadpour (2009) [17] | Linear superposition based on slip flow and Knudsen diffusion | Linear superposition; without consideration of real gas effect; only for nanopores with a circular cross-section |
| Azom and Javadpour (2012) [18] | Similar with Javadpour (2009) [17], real gas effect is considered | Linear superposition; only for nanopores with a circular cross-section |
| Darabi et al. (2012) [19] | Similar with Javadpour (2009) [17], the effect of wall roughness on Knudsen diffusion is considered | Linear superposition; without consideration of real gas effect; only for nanopores with a circular cross-section |
| Rahmanian et al. (2013) [20] | Weighted superposition based on continuum flow and Knudsen diffusion | Empirical parameters in determining weighted factors; without consideration of real gas effect; only for micro fractures |
| Singh et al. (2014) [21] | Linear superposition based on advective mass transfer and Knudsen diffusion | Linear superposition; without consideration of real gas effect |
| Wu et al. (2014) [8] | Weighted superposition based on slip flow and Knudsen diffusion | Without consideration of real gas effect; only for nanopores with a circular cross-section |
| Wu et al. (2015) [22] | Similar with Wu et al. (2014) [8], real gas effect is considered | Only for nanopores with a circular cross-section |
| Wu et al. (2015) [23] | Weighted superposition based on slip flow and Knudsen diffusion | Without consideration of real gas effect; only for micro fractures |

gas transport in nanopores with all cross-section types and shapes is complex and/or impossible [12,30,32]. Fortunately, the gas mass flux calculated by a unified model, which is a probabilistic combination based on gas transport model for nanopores with a circular and a rectangular cross section, can meet the engineering precision requirements in SGRs [21].

In this paper, firstly, a model for real gas transport is proposed by weighted superposition of slip flow and Knudsen diffusion. The present model not only considers slip effect and real gas effect, but also considers the effects of nanopores type, shape and size on gas transport. Second, the present model is validated with molecular simulation results published. Third, gas transport mechanisms are discussed, and effects of real gas effect, nanopores type, shape and size on gas transport are analyzed. Finally conclusions.

## 2. Model establishment

A model for gas transport is established on the basis of weighted superposition of slip flow and Knudsen diffusion, where the ratios of the gas intermolecular collisions and the gas molecule–nanopore wall collisions to the total collisions are the weighted factors of slip flow and Knudsen diffusion, respectively.

### 2.1. Ideal gas transport model for nanopores with a circular cross section

Mean free path for ideal gas can be expressed as [36]:

$$\lambda_i = \frac{\eta}{p}\sqrt{\frac{\pi RT}{2M}} \tag{1}$$

Knudsen number for ideal gas transport through nanopores can be expressed as [37]:

$$Kn_i = \frac{\lambda_i}{2r} \tag{2}$$

#### 2.1.1. Slip flow

When $10^{-3} < Kn_i < 10^{-1}$, compared with the gas intermolecular collision, the gas molecule–nanopore wall collision can't be neglected, and gas transport is governed by slip flow. Taking account of slip effect, slip flow mass flux for ideal gas through nanopores with a circular cross section is expressed as [38]:

$$J_{C-vsi} = -\frac{\phi}{\tau}\frac{r^2 pM}{8\eta RT}(1+\alpha_i Kn_i)\left(1+\frac{4Kn_i}{1-bKn_i}\right)\frac{dp}{dl} \tag{3}$$

where $\phi/\tau$ is the correcting factor of gas transport in nanopores of SGRs, dimensionless, and the detail is found in our published paper [22]; $b$ is gas slip constant, dimensionless. When the boundary condition is the first-order slip flow, $b = 0$; when the boundary condition is the second-order slip flow, $b = -1$; $\alpha_i$ is the rarefaction coefficient for ideal gas and expressed as:

$$\alpha_i = \alpha_o \frac{2}{\pi}\tan^{-1}(\alpha_1 Kn_i^{\beta}) \tag{4}$$

Eq. (3) shows that the slip effect becomes obvious and gas mass flux increases with an increasing Knudsen number; however, even if Knudsen number becomes very high, Eq. (3) cannot be degraded to a Knudsen diffusion equation, and cannot describe the Knudsen diffusion for ideal gas.

#### 2.1.2. Knudsen diffusion

When $Kn_i > 10$, the collision between gas molecule and nanopore wall is dominant, and gas transport is governed by Knudsen diffusion. Taking account of wall roughness, Knudsen diffusion mass flux for ideal gas through nanopores with a circular cross section is expressed as [19,39]:

$$J_{C-ki} = -\frac{2}{3}\frac{\phi}{\tau} r\delta^{D_f-2}\left(\frac{8M}{\pi RT}\right)^{0.5}\frac{dp}{dl} \tag{5}$$

Combination of Eqs. (3) and (5) shows that Knudsen diffusion mass flux is independent of gas viscosity and pressure, which is different from slip flow mass flux.

#### 2.1.3. Total gas mass flux

On the basis of weighted superposition of slip flow and Knudsen diffusion, where the ratios of intermolecular collisions and molecule–nanopore wall collisions to the total collisions are the weighted factors of slip flow and Knudsen diffusion, respectively, a total mass flux for ideal gas through nanopores with a circular cross section is expressed as:

$$\begin{aligned} J_{C-ti} &= \omega_{C-vsi} J_{C-vsi} + \omega_{C-ki} J_{C-ki} \\ \omega_{C-vsi} &= \tfrac{1}{(1+Kn_i)} \\ \omega_{C-ki} &= \tfrac{1}{(1+1/Kn_i)} \end{aligned} \tag{6}$$

where $\omega_{C\text{-}vsi}$ and $\omega_{C\text{-}ki}$ are weighted factors for slip flow and Knudsen diffusion through nanopores with a circular cross section for ideal gas, respectively, dimensionless. The detail for their derivations can be found in our published paper [22]. When pressure increases, the intermolecular collisions gradually dominate, gas transport is gradually controlled by slip flow, and the weighted factor $\omega_{C\text{-}vsi}$ for slip flow increases and approaches "1"; however, at the same time, the collisions between gas molecules and nanopores walls gradually weaken, Knudsen diffusion becomes less important, and the weighted factor $\omega_{C\text{-}ki}$ for Knudsen diffusion decreases and approaches "0".

When $Kn_i < 10^{-3}$, Eq. (6) reduces to the Hagen–Poiseuille equation and can describe continuum flow; when $10^{-3} < Kn_i < 10^{-1}$, Eq. (6) reduces to Eq. (3) and can describe slip flow; when $Kn_i > 10$, Eq. (6) reduces to Eq. (5) and can describe Knudsen diffusion; when $10^{-1} < Kn_i < 10$, intermolecular collisions and collisions between gas moles and nanopore walls are both important for gas transport, and this gas transport is named transition flow and described by Eq. (6).

### 2.2. Ideal gas transport model for nanopores with a rectangular cross section

Nanopores in SGRs are complex and generally nonequant in diameter of cross sections, with a varying aspect ratio from 1.8: 1.0 to 4.1: 1.0, and a mean aspect ratio of 2.8: 1.0 [40]. Some nanopores can be simplified to a plane with a rectangular cross section [20], as shown in Fig. 2, and the corresponding aspect ratio can be expressed as:

$$\zeta = \frac{w}{h} \tag{7}$$

Knudsen number is the ratio of the mean free path for ideal gas to the height of a rectangular cross section in nanopores [23,38], and can be expressed as:

$$Kn_i = \frac{\lambda_i}{h} \tag{8}$$

#### 2.2.1. Slip flow

When $10^{-3} < Kn_i < 10^{-1}$, compared with the gas intermolecular collision, the gas molecule–nanopore wall collision can't be neglected, and gas velocity isn't zero on nanopore wall. By correcting the slip boundary condition, slip flow mass flux for ideal gas

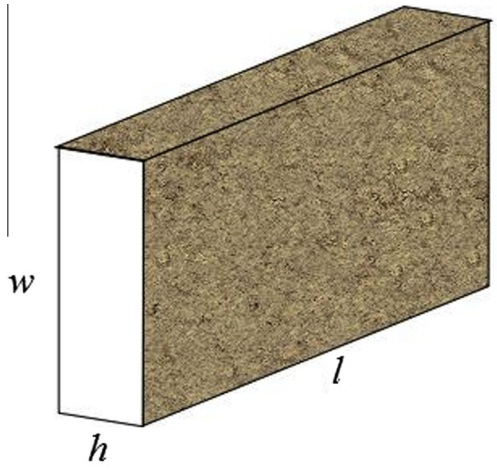


**Fig. 2.** Scenario of the simplified model for a nanopore with a rectangular cross-section.

through nanopores with a rectangular cross section is expressed as [23]:

$$J_{\mathrm{R-vsi}} = -A(\zeta)\frac{\phi}{\tau}\frac{h^2}{12\eta}\frac{pM}{RT}(1+\alpha_{\mathrm{i}}Kn_{\mathrm{i}})\left(1+\frac{6Kn_{\mathrm{i}}}{1-bKn_{\mathrm{i}}}\right)\frac{\mathrm{d}p}{\mathrm{d}l} \tag{9}$$

where

$$A(\zeta) = 1-\frac{192}{\zeta\pi^5}\sum_{i=1,3,5,\ldots}^{\infty}\frac{\tanh(i\pi\zeta/2)}{i^5} \tag{10}$$

where $A(\zeta)$ is the section shape factor of nanopores with a rectangular cross section for slip flow, dimensionless, and independent of Knudsen number. $A(\zeta)$ is a function of the aspect ratio of nanopores with a rectangular section, as shown in Fig. 3.

*2.2.2. Knudsen diffusion*

When $Kn_{\mathrm{i}} > 10$, the collision between gas molecule and nanopore wall is dominant, and gas transport is governed by Knudsen diffusion. Taking into account the cross-section type and shape, Knudsen diffusion mass flux for ideal gas through nanopores with a rectangular cross section is expressed as [23]:

$$J_{\mathrm{R-ki}} = -B(\zeta)\frac{\phi}{\tau}\frac{h^2}{w}\delta^{D_{\mathrm{f}}-2}\left(\frac{M}{2\pi RT}\right)^{0.5}\frac{\mathrm{d}p}{\mathrm{d}l} \tag{11}$$

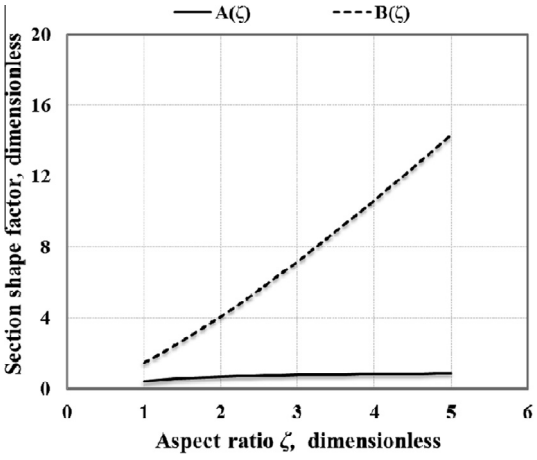


**Fig. 3.** The curves for section shape factor with aspect ratio.

where

$$B(\zeta) = \left\{\zeta^2\ln\left[\frac{1}{\zeta}+\sqrt{1+\frac{1}{\zeta^2}}\right]+\zeta\ln\left[\zeta+\sqrt{1+\zeta^2}\right]-\frac{(\zeta^2+1)^{3/2}}{3}+\frac{(1+\zeta^3)}{3}\right\} \tag{12}$$

where $B(\zeta)$ is the section shape factor of nanopores with a rectangular cross section for Knudsen diffusion, dimensionless, and independent of Knudsen number. $B(\zeta)$ is a function of the aspect ratio of nanopores with a rectangular section, as shown in Fig. 3.

*2.2.3. Total gas mass flux*

Similar to gas flow in nanopores with a circular cross section, a total mass flux for ideal gas in nanopores with a rectangular cross section is expressed as:

$$\begin{aligned} J_{\mathrm{R-ti}} &= \omega_{\mathrm{R-vsi}}J_{\mathrm{R-vsi}} + \omega_{\mathrm{R-ki}}J_{\mathrm{R-ki}} \\ \omega_{\mathrm{R-vsi}} &= \frac{1}{1+\frac{Kn_{\mathrm{i}}}{2}\left(1+\frac{1}{\zeta}\right)} \\ \omega_{\mathrm{R-ki}} &= \frac{1}{1+2/Kn_{\mathrm{i}}\left(1+\frac{1}{\zeta}\right)} \end{aligned} \tag{13}$$

where $\omega_{\mathrm{R\text{-}vsi}}$ and $\omega_{\mathrm{R\text{-}ki}}$ are weighted factors for slip flow and Knudsen diffusion through nanopores with a rectangular cross section for ideal gas, respectively, dimensionless. The detail for their derivations can be found in our published paper [23]. The varying characteristic of the weighted factors in pressure through nanopores with a rectangular cross section is similar to that of nanopores with a circular cross section.

Similar to Eq. (6), Eq. (13) for the total ideal gas mass flux is also able to describe continuum flow, slip flow, transition flow and Knudsen diffusion in nanopores with a rectangular cross section.

*2.3. Real gas transport model for nanopores*

Under a high pressure condition in SGRs, the gas intermolecular interaction force is very strong, which significantly affects gas transport. Additionally, the diameter of gas molecule is comparable with that of nanopores, and its volume also significantly affects gas transport. All mentioned above is named as real gas effect, and its effect on gas transport can be characterized by the real gas compressibility factor, viscosity and mean free path together.

Gas compressibility factor is a function of temperature and pressure, and can be expressed with a reduced temperature and a reduced pressure [41]:

$$\begin{aligned} Z &= 1+\frac{p_{\mathrm{r}}}{10.24T_{\mathrm{r}}}\left[2.16\frac{1}{T_{\mathrm{r}}}\left(\frac{1}{T_{\mathrm{r}}}+1\right)-1\right] \\ p_{\mathrm{r}} &= p/p_{\mathrm{c}} \\ T_{\mathrm{r}} &= T/T_{\mathrm{c}} \end{aligned} \tag{14}$$

Similarly, gas viscosity is also a function of temperature and pressure, and can be expressed as [42]:

$$\eta_{\mathrm{r}} = \eta\left[1+\frac{A_1}{T_{\mathrm{r}}^5}\left(\frac{p_{\mathrm{r}}^4}{T_{\mathrm{r}}^{20}+p_{\mathrm{r}}^4}\right)+A_2\left(\frac{p_{\mathrm{r}}}{T_{\mathrm{r}}}\right)^2+A_3\left(\frac{p_{\mathrm{r}}}{T_{\mathrm{r}}}\right)\right] \tag{15}$$

Mean free path for real gas can be expressed as [43]:

$$\lambda_{\mathrm{r}} = \frac{\eta_{\mathrm{r}}}{p}\sqrt{\frac{\pi ZRT}{2M}} \tag{16}$$

Knudsen numbers for real gas in nanopores with a circular cross section and a rectangular cross section are expressed, respectively.

$$Kn_{\mathrm{r}} = \frac{\lambda_{\mathrm{r}}}{2r} \tag{17}$$

$$Kn_{\mathrm{r}} = \frac{\lambda_{\mathrm{r}}}{h} \tag{18}$$

The rarefaction coefficient for real gas is expressed as:

$$\alpha_r = \alpha_o \frac{2}{\pi} \tan^{-1}\left(\alpha_1 Kn_r^{\beta}\right) \tag{19}$$

#### 2.3.1. Slip flow

Respectively, according to Eqs. (3) and (9), slip flow mass flux for real gas in nanopores with a circular cross section and rectangular cross section can be expressed as:

$$J_{C-vsr} = -\frac{\phi}{\tau}\frac{r^2}{8\eta_r}\frac{pM}{ZRT}(1+\alpha_r Kn_r)\left(1+\frac{4Kn_r}{1-bKn_r}\right)\frac{dp}{dl} \tag{20}$$

$$J_{R-vsr} = -A(\zeta)\frac{\phi}{\tau}\frac{h^2}{12\eta_r}\frac{pM}{ZRT}(1+\alpha_r Kn_r)\left(1+\frac{6Kn_r}{1-bKn_r}\right)\frac{dp}{dl} \tag{21}$$

#### 2.3.2. Knudsen diffusion

Respectively, according to Eqs. (5) and (11), Knudsen diffusion mass flux for real gas in nanopores with a circular cross section and rectangular cross section can be expressed as:

$$\begin{aligned} J_{C-kr} &= -\frac{2}{3}\frac{\phi}{\tau} r \delta^{D_f-2}\left(\frac{8ZM}{\pi RT}\right)^{0.5}\frac{p}{Z}C_g\frac{dp}{dl} \\ C_g &= \frac{1}{p}-\frac{1}{Z}\frac{dZ}{dp} \end{aligned} \tag{22}$$

$$J_{R-kr} = -B(\zeta)\frac{\phi}{\tau}\frac{h^2}{w}\delta^{D_f-2}\left(\frac{ZM}{2\pi RT}\right)^{0.5}\frac{p}{Z}C_g\frac{dp}{dl} \tag{23}$$

#### 2.3.3. Total gas mass flux

Similar with ideal gas, on the basis of weighted superposition of slip flow and Knudsen diffusion with the corresponding Eqs. (20) and (22), a total mass flux for real gas in nanopores with a circular cross section is expressed as:

$$J_{C-tr} = \omega_{C-vsr} J_{C-vsr} + \omega_{C-kr} J_{C-kr} \tag{24}$$

Similarly, a total mass flux for real gas in nanopores with a rectangular cross section is expressed as:

$$J_{R-tr} = \omega_{R-vsr} J_{R-vsr} + \omega_{R-kr} J_{R-kr} \tag{25}$$

Similar to Eqs. (6) and (13), Eqs. (24) and (25) for the total real gas mass flux are also able to describe continuum flow, slip flow, transition flow and Knudsen diffusion in nanopores with a circular cross section and rectangular cross section, respectively. Additionally, these real gas transport models consider the effect of real gas on gas transport in nanopores of SGRs.

## 3. Model validation

Molecular Simulation data is accurate and often used to verify the model for gas transport in nanopores; on the contrary, experiment results are less applied to model validation, because experiment cannot accurately reflect the ideal conditions for a theoretical model [44,45]. Therefore, the present model is validated by comparing the results calculated by the present model with molecular simulation data published.

Modeling parameters are listed in Table 2.

### 3.1. Validation of ideal gas transport model for nanopores

For the convenience of comparison, based on continuum flow mass flux and Knudsen diffusion mass flux, the total mass flux for ideal gas in nanopores with a circular cross section is normalized as, respectively:

$$\begin{aligned} \frac{J_{C-ti}}{J_{C-vi}} &= \omega_{C-vsi}(1+\alpha_i Kn_i)\left(1+\frac{4Kn_i}{1-bKn_i}\right)+\omega_{C-ki}\delta^{D_f-2}Kn_i\frac{128}{3\pi} \\ J_{C-vi} &= -\frac{\phi}{\tau}\frac{r^2 pM}{8\eta RT}\frac{dp}{dl} \end{aligned} \tag{26}$$

$$\frac{J_{C-ti}}{J_{C-ki}} = \omega_{C-vsi}(1+\alpha_i Kn_i)\left(1+\frac{4Kn_i}{1-bKn_i}\right)\frac{3\pi}{128\delta^{D_f-2}Kn_i}+\omega_{C-ki} \tag{27}$$

where $J_{C\text{-}ti}/J_{C\text{-}vi}$ is the dimensionless ideal gas flux based on continuum flow mass flux through nanopores with a circular crosssection, dimensionless; $J_{C\text{-}ti}/J_{C\text{-}ki}$ is the dimensionless ideal gas flux based on Knudsen diffusion mass flux through nanopores with a circular cross section, dimensionless.

Fig. 4 shows that the analytic solutions calculated by the present model for ideal gas transport in nanopores with a circular cross section are in good agreement with the molecular simulation data published, which demonstrates that the present model is reliable to model the rarefied gas transport at a low pressure.

For the validation of ideal gas transport model in nanopores with a rectangular cross section, similar to that in nanopores with

**Table 2**
Summary of modeling parameters in the calculation.

| Parameter | Symbol | Unit | Value |
|---|---|---|---|
| Porosity | $\phi$ | Decimal | 0.05 |
| Tortuosity | $\tau$ | Dimensionless | 4.3 |
| Nanopores radius | $r$ | $m$ | $2.0\times10^{-9}\sim1.0\times10^{-6}$ |
| Aspect ratio for nanopores with a rectangular cross-section | $\zeta$ | dimensionless | 1, 2, 4 |
| Nitrogen molar mass | $M$ | kg/mol | $2.80\times10^{-2}$ |
| Nitrogen viscosity ($p$ = 0.101325 MPa, $T$ = 423 K) | $\eta$ | $P_a$ s | $2.31\times10^{-5}$ |
| Critical pressure of nitrogen | $p_c$ | MPa | 3.39 |
| Critical temperature of nitrogen | $T_c$ | K | 126.2 |
| Methane molar mass | $M$ | kg/mol | $1.60\times10^{-2}$ |
| Methane viscosity ($p$ = 0.101325 MPa, $T$ = 423 K) | $\eta$ | $P_a$ s | $1.49\times10^{-5}$ |
| Critical pressure of methane | $p_c$ | MPa | 4.60 |
| Critical temperature of methane | $T_c$ | K | 190.6 |
| Universal gas constant | $R$ | J/(mol K) | 8.314462 |
| Temperature | $T$ | K | 423 |
| Rarefaction coefficient at $K_n\to\infty$ | $\alpha_0$ | Dimensionless | 1.19 |
| Fitting constant | $\alpha_1$ | Dimensionless | 4.0 |
| Fitting constant | $\beta$ | Dimensionless | 0.4 |
| Gas slip constant | $b$ | Dimensionless | −1 |
| Ratio of normalized molecule size to local average pore diameter | $\sigma$ | Dimensionless | 0.5 |
| Fractal dimension of the pore wall | $D_f$ | Dimensionless | 2.5 |
| Fitting constant | $A_1$ | Dimensionless | 7.9 |
| Fitting constant | $A_2$ | Dimensionless | $9.0\times10^{-6}$ |
| Fitting constant | $A_3$ | Dimensionless | 0.28 |

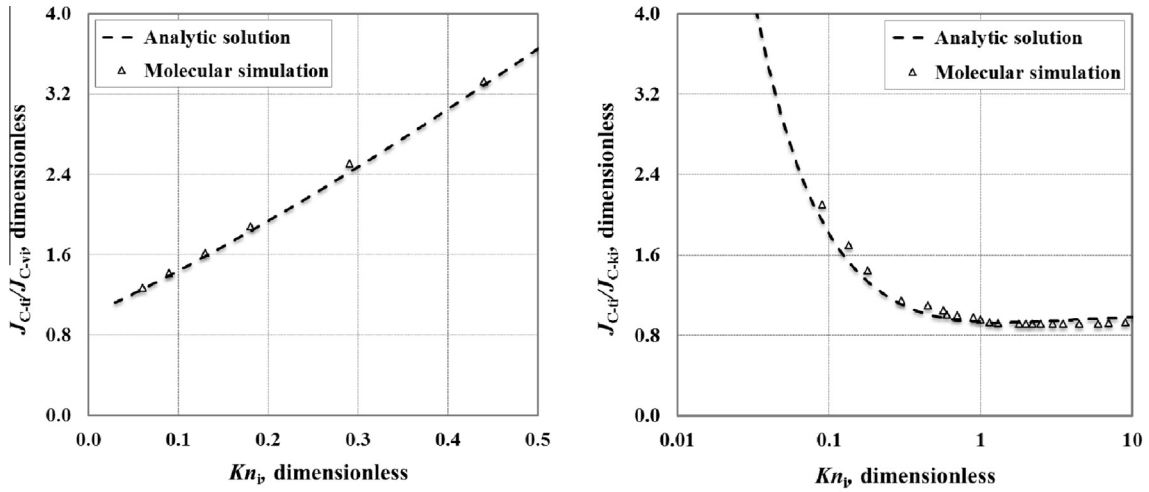


(a) $J_{C\text{-}ti}/J_{C\text{-}vi} \sim Kn_i$ (b) $J_{C\text{-}ti}/J_{C\text{-}ki} \sim Kn_i$

**Fig. 4.** Comparison of analytic solutions and molecular simulation data for ideal gas in nanopores with a circular section. *Note:* The Legend "Molecular simulation" is the data for rarefied gas transfer under low pressure simulated by Loyalka and Hamoodi [46].

a circular cross section, based on continuum flow mass flux and Knudsen diffusion mass flux, the total mass flux for ideal gas in nanopores with a rectangular cross section is normalized as, respectively:

$$\frac{J_{R-ti}}{J_{R-vi}} = \omega_{R-vsi} A(\zeta)(1+\alpha_i Kn_i)\left(1+\frac{6Kn_i}{1-bKn_i}\right) + \omega_{R-ki}\delta^{D_f-2}\frac{12Kn_i}{\pi}\frac{B(\zeta)}{\zeta}$$
$$J_{R-vi} = -\frac{\phi}{\tau}\frac{h^2}{12\eta}\frac{pM}{RT}\frac{dp}{dl} \tag{28}$$

$$\frac{J_{R-ti}}{J_{R-ki}} = \omega_{R-vsi}\frac{\pi}{12\delta^{D_f-2}Kn_i}\zeta A(\zeta)(1+\alpha_i Kn_i)\left(1+\frac{6Kn_i}{1-bKn_i}\right) + \omega_{R-ki}B(\zeta) \tag{29}$$

where $J_{R\text{-}ti}/J_{R\text{-}vi}$ is the dimensionless ideal gas flux based on continuum flow flux through nanopores with a rectangular cross section, dimensionless; $J_{R\text{-}ti}/J_{R\text{-}ki}$ is the dimensionless ideal gas flux based on Knudsen diffusion flux through nanopores with a rectangular cross section, dimensionless.

For ideal gas transport in nanopores with the rectangular cross section of different aspect ratios, results calculated by the present model have good agreement with molecular simulation data, suggesting that the present model can describe the ideal gas transport behavior, as shown in Fig. 5.

Figs. 4(b) and 5(b) both show that, for gas transport in nanopores with either a rectangular or a circular cross section, there is always a minimum gas transport capacity over the whole range of Knudsen number, i.e., at $Kn_i = 1$, the dimensionless ideal gas flux approaches to the minimum value, which is consistent with the results obtained by scholars with the Molecular Simulation or experiments [46–51]. In other words, gas transport capacity firstly decreases and then gradually increases with an increasing Knudsen number, which is also consistent with the practical phenomenon that gas flux decreases slowly in the later period of production in SGRs [52].

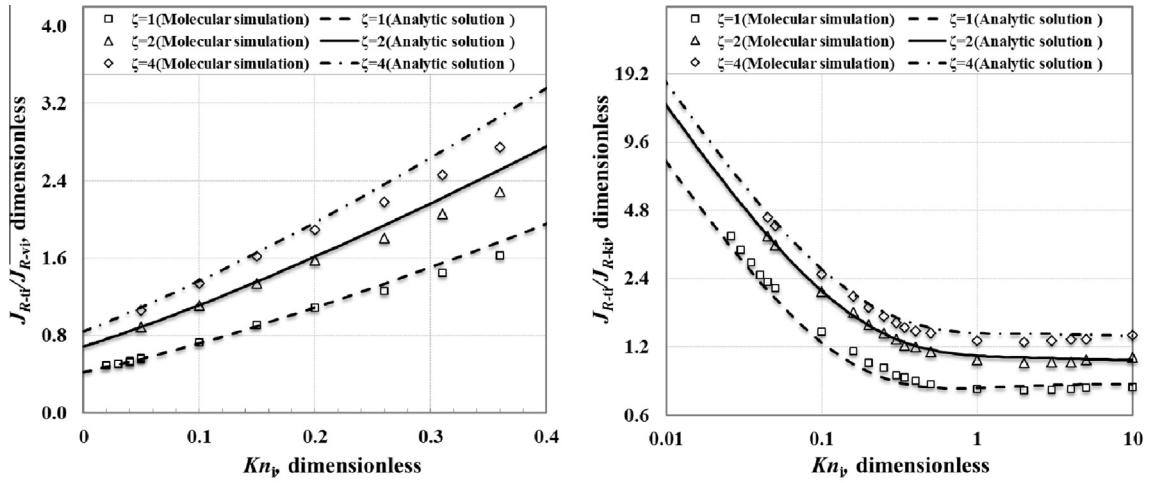


(a) $J_{R\text{-}ti}/J_{R\text{-}vi} \sim Kn_i$ (b) $J_{R\text{-}ti}/J_{R\text{-}ki} \sim Kn_i$

**Fig. 5.** Comparison of analytic solutions and molecular simulation data for ideal gas in nanopores with a rectangular section. *Note:* The Legend "Molecular simulation" is the data obtained by Sone and Hasegawa with a linear lattice Boltzmann method [47].

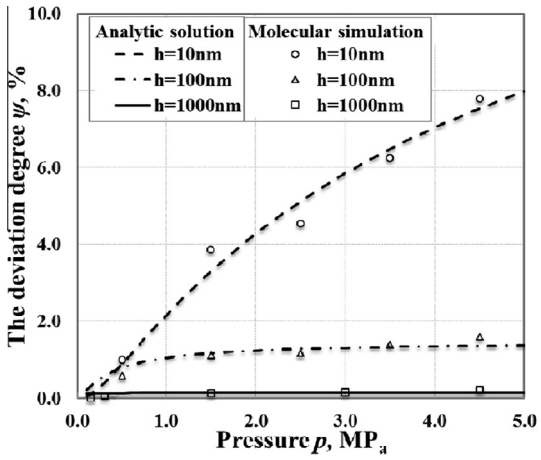


**Fig. 6.** Comparison of analytic solutions and molecular simulation data of $\psi$ with $p$ for nitrogen transfer in nanopores with different $h$ of a rectangular section. *Note:* The Legend "Molecular simulation" is the gas transfer data at a relatively high pressure modeled by Wang and Li with the direct simulation Monte Carlo method [53].

### 3.2. Validation of real gas transport model for nanopores

For the convenience of validation, only take the model for real gas transport in nanopores with a rectangular cross section as an example, additionally, the present model is validated by comparing the deviation degree between gas mass flux calculated by ideal gas model and real gas model with that obtained by the molecular simulation data published. The deviation degree can be expressed as:

$$\psi = (J_{R-tr} - J_{R-ti}) \times 100\%/J_{R-ti} \tag{30}$$

Fig. 6 shows that analytic solutions calculated by the present model are consistent with the molecular simulation data published, indicating that the present model for real gas transport can reasonably model gas transport behavior in nanopores at a relatively high pressure.

## 4. Results and discussion

Based on the results calculated by the present model, Firstly, gas transport behavior in nanopores is elaborated; then analyze the role of real gas effect on gas transport in nanopores; and finally the impacts of nanopores type, shape and size on gas transport are discussed.

For the convenience of discussion, the gas transport capacity in nanopores with different cross sections is expressed by a conductance.

According to Eq. (6), total conductance for ideal gas through nanopores with a circular cross section is:

$$\begin{aligned} C_{C-ti} &= C_{C-vsi} + C_{C-ki} \\ &= \frac{1}{(1+Kn_i)}\frac{\phi}{\tau}\frac{r^2 pM}{8\eta RT}(1+\alpha_i Kn_i)\left(1+\frac{4Kn_i}{1-bKn_i}\right) \\ &\quad + \frac{1}{(1+1/Kn_i)}\frac{2}{3}\frac{\phi}{\tau} r\delta^{D_f-2}\left(\frac{8M}{\pi RT}\right)^{0.5} \end{aligned} \tag{31}$$

According to Eq. (24), total conductance for real gas through nanopores with a circular cross section is:

$$\begin{aligned} C_{C-tr} &= C_{C-vsr} + C_{C-kr} \\ &= \frac{1}{(1+Kn_r)}\frac{\phi}{\tau}\frac{r^2 pM}{8\eta_r RTZ}(1+\alpha_r Kn_r)\left(1+\frac{4Kn_r}{1-bKn_r}\right) \\ &\quad + \frac{1}{(1+1/Kn_r)}\frac{2}{3}\frac{\phi}{\tau} r\delta^{D_f-2}\left(\frac{8ZM}{\pi RT}\right)^{0.5}\frac{p}{Z}C_g \end{aligned} \tag{32}$$

According to Eq. (13), total conductance for ideal gas through nanopores with a rectangular cross section is:

$$\begin{aligned} C_{R-ti} &= C_{R-vsi} + C_{R-ki} \\ &= \frac{1}{1+\frac{Kn_i}{2}\left(1+\frac{1}{\zeta}\right)}A(\zeta)\frac{\phi}{\tau}\frac{h^2}{12\eta}\frac{pM}{RT}(1+\alpha_i Kn_i)\left(1+\frac{6Kn_i}{1-bKn_i}\right) \\ &\quad + \frac{1}{1+2/Kn_i\left(1+\frac{1}{\zeta}\right)}B(\zeta)\frac{\phi}{\tau}\frac{h^2}{w}\delta^{D_f-2}\left(\frac{M}{2\pi RT}\right)^{0.5} \end{aligned} \tag{33}$$

According to Eq. (25), total conductance for real gas through nanopores with a rectangular cross section is:

$$\begin{aligned} C_{R-tr} &= C_{R-vsr} + C_{R-kr} \\ &= \frac{1}{1+\frac{Kn_r}{2}\left(1+\frac{1}{\zeta}\right)}A(\zeta)\frac{\phi}{\tau}\frac{h^2}{12\eta_r}\frac{pM}{ZRT}(1+\alpha_r Kn_r)\left(1+\frac{6Kn_r}{1-bKn_r}\right) \\ &\quad + \frac{1}{1+2/Kn_r\left(1+\frac{1}{\zeta}\right)}B(\zeta)\frac{\phi}{\tau}\frac{h^2}{w}\delta^{D_f-2}\left(\frac{ZM}{2\pi RT}\right)^{0.5}\frac{p}{Z}C_g \end{aligned} \tag{34}$$

### 4.1. Gas transport behavior in nanopores

Gas transport mechanisms include continuum flow, slip flow and transition flow in nanopores of SGRs. In this paper, coupling slip flow and Knudsen diffusion describes these transport mechanisms.

Fig. 7 is the comparisons of slip flow conductance, Knudsen diffusion conductance and total conductance for real gas in nanopores with a circular cross section and a rectangular cross section at the same cross-sectional area. Slip flow conductance decreases with a decreasing pressure, as shown in Fig. 7a. Although slip effect enhances slip flow conductance to some extent, however, slip flow is proportional to pressure, and its weighted factor decreases with a decreasing pressure (shown in Eqs. (32) and (34)), which is caused that slip flow conductance decreases with a decreasing pressure; on the contrary, Knudsen diffusion conductance increases with a decreasing pressure, as shown in Fig. 7b. This is because that Knudsen diffusion itself is not sensitive to pressure, but its weighted factor increases sharply with a decreasing pressure (shown in Eqs. (32) and (34)); a total conductance firstly decreases and then gradually increases with a decreasing pressure in nanopores, as shown in Fig. 7c. This is because that slip flow dominates gas transport at a high pressure, and Knudsen diffusion governs gas transport at a low pressure, which is also one of reasons that gas well deliverability decreases slowly in the later period of production in SGRs [52].

Fig. 7 shows that nanopores type and shape affect gas transport: (1) gas transport capacity in nanopores with a circular cross section is stronger than that in nanopores with a rectangular cross section, gas transport capacity in nanopores with a rectangular cross section decreases with an increasing aspect ratio; (2) compared with nanopores type, the effect of nanopores shape (varying aspect ratio) on gas transport is greater [54].

Nanopores type and shape affect gas transport mechanism and capacity, which can be explained from the microscopic point of view: (1) the interaction force between wall solid molecules and gas molecules is different from the gas intermolecular force, which causes the difference of gas molecules number density between the wall vicinity and away from the wall [34,35]; (2) gas molecules near wall prematurely collide with wall, which drastically reduces the mean free path [33]; (3) nanopores with different type and shape have different specific surface, which causes different ratios of the gas molecules–wall collision frequency to the total collision frequency [31]. In addition, this phenomenon can also be explained

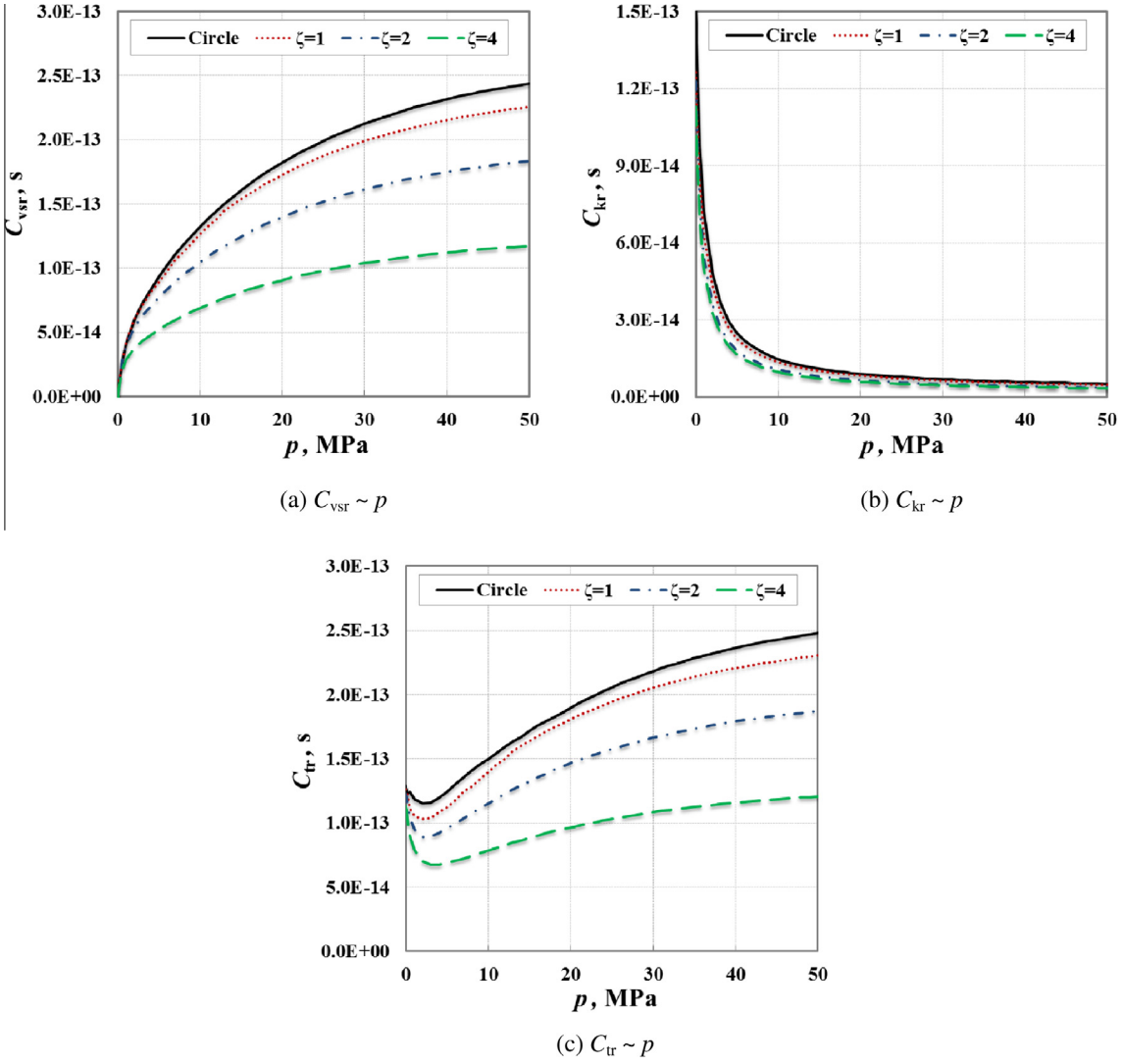


**Fig. 7.** Different transport conductance with pressure for real gas ($S$ = 78.54 nm$^2$, $r$ = 5 nm, $T$ = 423 K).

from a macro point of view. For example, for slip flow, gas slip velocity is related to local wall shear stress, and shear stress is a function of nanopores wall property, type and shape. Therefore, nanopores type and shape affect slip flow [32]. The cross-sectional area and perimeter of nanopores are key parameters that affect slip flow [12,30,32]. Gas transport is governed by Knudsen diffusion in nanopores with a radius less than or equal 5 nm at a low pressure [55]. For Knudsen diffusion, the quantitative research is rare in the effect of nanopores type and shape on gas transport capacity [56]. Eldridge and Brown (1976) indicated that Knudsen diffusion coefficient in nanopores with a rectangular cross section of an aspect ratio of 3.5 is smaller 10% than that in nanopores with a circular cross section [57], which is consistent with results in this paper.

Fig. 7 also shows that for gas transport in nanopores with a rectangular cross section of the larger aspect ratio, total conductance decrease more slowly in early period of depressurization and increases more quickly in later period of depressurization [29,58]. This is due to the larger the Knudsen number, the stronger the slip effect, and the larger the share of Knudsen diffusion to all gas transport mechanisms for gas transport in nanopores with a rectangular cross section of the larger aspect ratio. The similar result was also presented by Morini et al. (1998, 2004) with the numerical simulation method [59,60].

The ratio of total conductance to continuum flow conductance with pressure in nanopores with a circular cross section and a rectangular cross section is shown in Fig. 8. The figure shows that: (1) the ratio increases with a decreasing pressure. This is because the mean free path increases, slip effect enhances, and Knudsen diffusion gradually governs gas transport when pressure decreases; (2) compared with nanopores with a circular cross section, the ratio for nanopores with a rectangular cross section is larger, and it increases with an increasing aspect ratio. This is due to the smaller the pore characteristic length, the larger the share of Knudsen layer to the pore characteristic length, the stronger the collisions between gas molecules–wall, and the stronger the slip effect in nanopores with a rectangular cross section of the larger aspect ratio [33,61]. The similar result was also presented by Morini et al. (2004) with the numerical simulation method [60].

### 4.2. Real gas effect of gas transport in nanopores

In nanopores of SGRs, real gas effect significantly influences gas transport, and the reasons are that: (1) a gas molecule cannot be assumed as a point, because its diameter is comparable with nanopore diameter, which reduces the gas transport capacity and cannot be ignored [62]; (2) at a low pressure, the gas intermolecular force is attractive force, which decreases mean free path, weakens

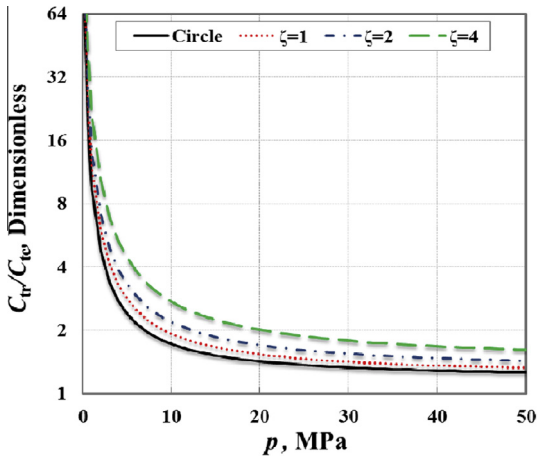


**Fig. 8.** The ratio of total conductance to continuum flow conductance with pressure ($S$ = 78.54 nm$^2$, $r$ = 5 nm, $T$ = 423 K).

slip effect, and reduces gas transport capacity [33]; (3) on the contrary, at a high pressure, the gas intermolecular force is repulsive force, which increases mean free path, strengthens slip effect, and enhances gas transport capacity [33].

The deviation degree between real gas conductance and ideal gas conductance with pressure is shown in Fig. 9. The figure shows that: (1) the transport capacity of real gas is stronger than that of ideal gas. This is due to the gas intermolecular repulsive force at a high pressure in nanopores of SGRs; (2) compared with nanopores with a circular cross section, the deviation degree is larger in nanopores with a rectangular cross section, and it increases with an increasing aspect ratio. This is because that there is the smaller the pore characteristic length, the larger the Knudsen number and the stronger the slip effect in nanopores with a rectangular cross section of the larger aspect ratio, and real gas effect further strengthens the influences of slip effect and Knudsen diffusion on gas transport capacity; (3) comparison of Fig. 9a and b indicates that, compared with slip flow, the deviation degree of Knudsen diffusion conductance is larger. This is because that Knudsen diffusion is more dependent on the collisions between gas molecules and wall, and real gas effect enhances the collisions at a high pressure.

Fig. 9c shows that real gas effect enhances gas transport capacity by 14.2% ~ 29.5% in nanopores with a cross-sectional area of 78.54 nm$^2$ at a pressure of 50 MPa, which is consistent with research findings published. Wang and Li (2008) modeled gas transport mechanism in micro and nano-scale pores by the direct simulation Monte Carlo method, and concluded that real gas effect enhances gas transport capacity by 28.6% in a nano-scale pore with a height of 10 nm at a pressure of 4.4 MPa [63]; Michel et al. (2011) also presented that real gas effect enhances gas transport capacity by 60.0% in nanopores with a radius of 5 nm at a pressure of 99.97 MPa in SGRs [64]; based on Javadpour model [17], Ma

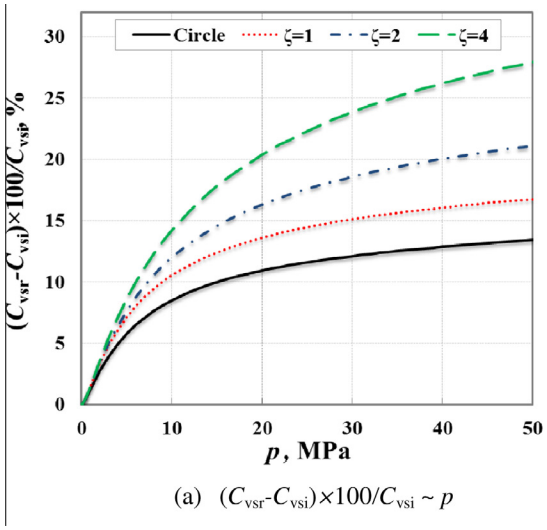


(a) $(C_{vsr}-C_{vsi})\times100/C_{vsi} \sim p$

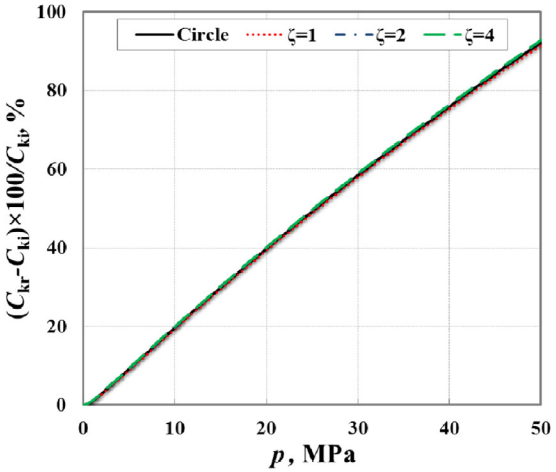


(b) $(C_{kr}-C_{ki})\times100/C_{ki} \sim p$

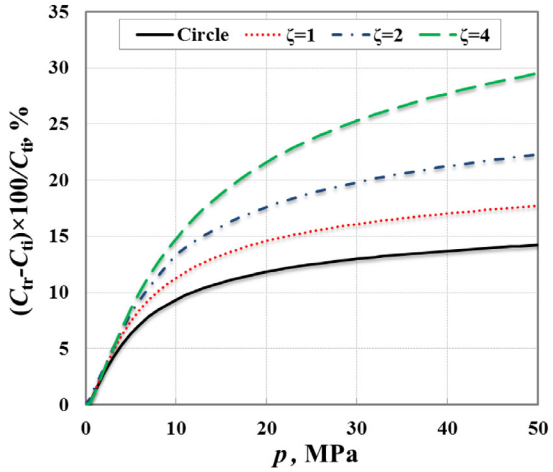


(c) $(C_{tr}-C_{ti})\times100/C_{ti} \sim p$

**Fig. 9.** Deviation degree with pressure for different transport mechanisms ($S$ = 78.54 nm$^2$, $r$ = 5 nm, $T$ = 423 K).

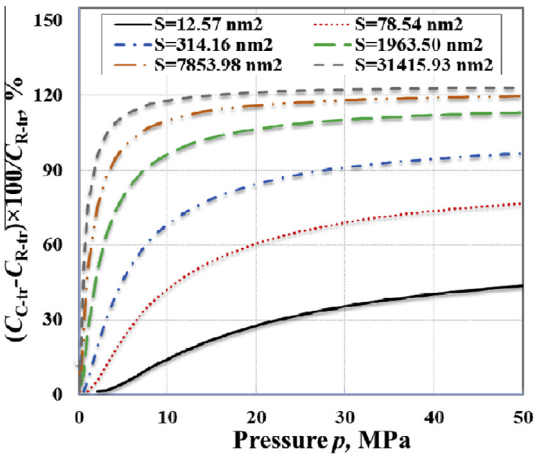


**Fig. 10.** Deviation degree of real gas transport conductance between circular and rectangular cross-section nanopores with pressure for different nanopore scales ($\zeta = 4$ for nanopores with a rectangular cross-section).

et al. (2014) derived a model of real gas transport through nanopores with a circular cross section, and indicated gas transport capacity enhanced by 10.0% due to real gas effect [65]; Wu et al. (2015) indicated that the real gas effect influences gas transport most, up to 12.76% in SGRs with a temperature of 423 K and relative low pressure ($p \leqslant 22$ MPa) [66]. With all mentioned above, the impact of real gas effect on gas transport is not negligible in nanopores of SGRs.

### 4.3. Sensitivity of nanopores dimension on gas transport

The deviation degree between real gas conductance in nanopores with a circular cross section and that in nanopores with a rectangular cross section with pressure is shown in Fig. 10. The figure shows that real gas conductance in nanopores with a circular cross section is higher than that in nanopores with a rectangular cross section, and the deviation degree increases with increasing pressure and pore size. At a pressure of 50 MPa, the deviation degree increases from 43.5% to 123.1% when the cross-sectional area increases from 12.57 $nm^2$ to 31415.93 $nm^2$. This is because (1) at a high pressure, gas transport is mainly governed by slip flow, and its share over all gas transport mechanisms increases with increasing pressure and pore size; (2) The difference is large between slip flow conductance in nanopores with a circular cross section and that in nanopores with a rectangular cross section (Fig. 7a), however, small difference in Knudsen diffusion conductance (Fig. 7b).

Fig. 11a and b are the deviation degree of transport conductance between real gas and ideal gas with pressure in nanopores with a circular cross section and with a rectangular cross section, respectively. The figures show that: (1) real gas effect enhances gas transport capacity; (2) the effect becomes strong with an increasing pressure and a decreasing pore size. This is because the greater the pressure, the larger the gas intermolecular repulsive force, the greater the mean free path and the stronger the slip effect; and the smaller the pore size and the smaller the pore characteristic length, which further amplifies the influence of real gas effect on gas transport. Comparison of Fig. 11a and b shows that compared with that in nanopores with a circular cross section, the influence of real gas effect on gas transport capacity is more obvious in nanopores with a rectangular cross section at the same cross-sectional area. At a cross-sectional area of 12.57 $nm^2$ and a pressure of 50 MPa, the deviation degree of transport conductance between real gas and ideal gas in nanopores with a circular cross section and with a rectangular cross section are up to 30.7% and 55.0%, respectively.

The two nanopore types considered in our models are nanopores with the circular and rectangular cross sections. When a shale matrix is composed of other nanopore types, the conductance of the shale matrix will be somewhere between those of these two types. Therefore, the two nanopore types considered in our models can reliably capture the average effect of different nanopore types in a shale matrix. Furthermore, capturing the exact type and shape of each nanopore might be impractical and difficult through the current laboratory experiment techniques. Additionally, finding analytical solutions for gas transport in nanopores with all cross-section types and shapes is complex and impossible [12,30,32]. Fortunately, the gas mass flux calculated by a unified model, which is a probabilistic combination based gas transport model for nanopores with a circular and a rectangular cross section, can meet the engineering precision requirements in SGRs [21]. For example, according to the SEM and AFM images of a shale matrix, if we approximate *x*% of nanopore types in these images as nanopores with a rectangular cross section and *y*% of

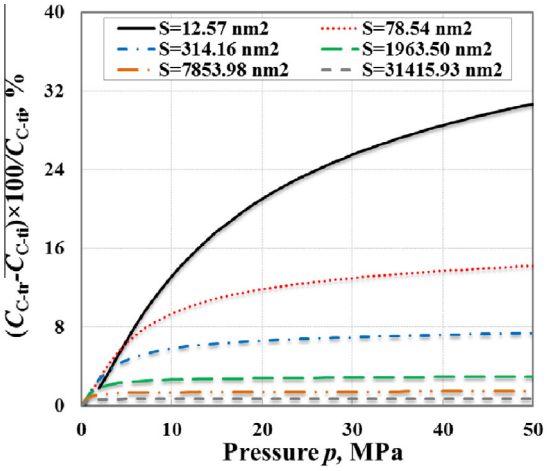


(a) gas transfer in nanopores with a circular cross-section

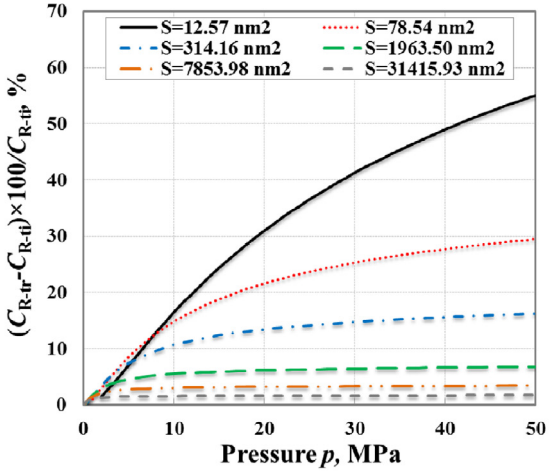


(b) gas transfer in nanopores with a rectangular cross-scetion

**Fig. 11.** Deviation degree of transport conductance between real gas and ideal gas with pressure for different pore size ($\zeta = 4$ for nanopores with a rectangular cross-section).

nanopore types as nanopores with a circular cross section, for the remaining nanopores types that do not match nanopores with the rectangular and circular cross sections, the apparent gas conductance of the shale matrix can be calculated as [21]:

$$C_{app-tr} = \frac{x}{100}C_{R-tr} + \frac{y}{100}C_{C-tr} + \left(\frac{100-x-y}{100}\right)\left(\frac{C_{R-tr}+C_{C-tr}}{2}\right) \quad (35)$$

Therefore, the circular and rectangular nanopore types used in the present model are enough to represent the real complex nanopore structure, and the present model can effectively upscale the gas conductance to a core scale in SGRs.

## 5. Conclusions

A unified model for gas transport was proposed on the basis of weighted superposition of slip flow and Knudsen diffusion in nanopores of SGRs. The present model takes into account slip effect and real gas effect, additionally, the effects of nanopore type, shape and size on gas transport are also considered. The present model was validated with the molecular simulation data published, and it can model gas transport behavior for different gas transport mechanisms in nanopores (with a circular and a rectangular cross section) of SGRs. Through analysis and discussion of the modeling results, the following conclusions can be drawn.

(1) Slip flow conductance decreases with a decreasing pressure; on the contrary, Knudsen diffusion conductance increases with a decreasing pressure; and a total conductance firstly decreases and then gradually increases with a decreasing pressure in nanopores, which is also one of reasons that gas well deliverability decreases slowly in the later period of production in SGRs.
(2) Nanopore type and shape affect gas transport: at the same cross-sectional area, gas transport capacity in nanopores with a circular cross section is greater than that in nanopores with a rectangular cross section, furthermore, the gas transport capacity in nanopores with a rectangular cross section decreases with an increasing aspect ratio; compared with nanopore type, the impact of nanopore shape on gas transport capacity is greater; the larger the aspect ratio for nanopores with a rectangular cross section, the more slowly the gas transport capacity decreases during the depressurization development in SGRs.
(3) Real gas effect enhances gas transport capacity, which increases with an increasing pressure and a decreasing pore size in nanopores of SGRs. Compared with that in nanopores with a circular section, the effect of real gas effect on gas transport capacity in nanopores with a rectangular cross section is stronger, and it increases with an increasing aspect ratio; the effect of real gas effect on Knudsen diffusion is greater compared with slip flow.

In this paper, the present model only considers the mass transport of free gas, without considering surface diffusion and desorption of adsorbed gas in nanopores of SGRs. Wherein the adsorption/desorption, resulting in only change of gas phase (the conversion between free gas and adsorbed gas), has no contribution to gas transport, but influences the adsorbed gas concentration and adsorption layer thickness, which both affect surface diffusion for adsorbed gas and gas transport for free gas in nanopores of SGRs [11,22].

## Acknowledgments

The authors would like to acknowledge the NSERC/AIEES/Foundation CMG and AITF Chairs for providing research funding. The first author also acknowledges the National Science and Technology Major Project of China (No. 2011ZX05030-005-04) and National Natural Science Foundation of China (No. 51490654 and No. 51374222) to support part of this work.

## References

[1] Y. Dai, J.R. Johnson, O. Karvan, D.S. Sholl, W.J. Koros, Ultem®/ZIF-8 mixed matrix hollow fiber membranes for $CO_2/N_2$ separations, J. Membr. Sci. 401 (2012) 76–82.
[2] M. Yoshimune, T. Yamamoto, M. Nakaiwa, K. Haraya, Preparation of highly mesoporous carbon membranes via a sol–gel process using resorcinol and formaldehyde, Carbon 46 (2008) 1031–1036.
[3] J.C. Liu, J. Wei, Knudsen diffusion in channels and networks, Chem. Eng. Sci. 111 (2014) 1–14.
[4] J.H. Petropoulos, K.G. Papadokostaki, May the Knudsen equation be legitimately, or at least usefully, applied to dilute adsorbable gas flow in mesoporous media, Chem. Eng. Sci. 68 (2012) 392–400.
[5] X. Guo, C. Huang, A. Alexeenko, J. Sullivan, Numerical and experimental study of gas flows in 2D and 3D microchannels, J. Micromech. Microeng. 18 (2008) 1–8.
[6] N.D. Stevanovic, A new analytical solution of microchannel gas flow, J. Micromech. Microeng. 17 (2007) 1695–1702.
[7] Y. Wu, J. Li, D. Ding, C. Wang, Y. Di, A generalized framework model for the simulation of gas production in unconventional gas reservoirs, SPE J. 19 (2014) 845–857.
[8] K. Wu, X. Li, C. Wang, W. Yu, C. Guo, D. Ji, Z. Chen, Apparent permeability for gas flow in shale reservoirs coupling effects of gas diffusion and desorption, in: SPE/AAPG/SEG Unconventional Resources Technology Conference, Denver, Colorado, USA, 2014.
[9] M.E. Curtis, C.H. Sondergeld, R.J. Ambrose, Microstructural investigation of gas shales in two and three dimensions using nanometer-scale resolution imaging, AAPG Bull. 96 (2012) 665–677.
[10] C. Guo, J. Xu, K. Wu, M. Wei, S. Liu, Study on gas flow through nano pores of shale gas reservoirs, Fuel 143 (2015) 107–117.
[11] K. Wu, X. Li, C. Wang, W. Yu, Z. Chen, A model for surface diffusion of adsorbed gas in nanopores of shale gas reservoirs, Ind. Eng. Chem. Res. 54 (2015) 3225–3236.
[12] M. Bahrami, M.M. Yovanovich, J.R. Culham, A novel solution for pressure drop in singly connected microchannels of arbitrary cross section, Int. J. Heat Mass Transfer 50 (2007) 2492–2502.
[13] R.W. Barber, D.R. Emerson, Challenges in modeling gas-phase flow in microchannels: from slip to transition, Heat Transfer Eng. 27 (2006) 3–12.
[14] C.A.S. Colin, High-order boundary conditions for gaseous flows in rectangular microducts, Microscale Thermophys. Eng. 5 (2001) 41–54.
[15] T. Ertekin, G. King, F. Schwerer, Dynamic gas slippage: a unique dual-mechanism approach to the flow of gas in tight formations, SPE Formation Eval. 1 (1986) 43–52.
[16] Q. Liu, B. Liu, X. Li, S. Yan, The effect of water saturation on gas slip factor by pore scale network modeling, in: SCA Symposium, Monterey, California, 2002.
[17] F. Javadpour, Nanopores and apparent permeability of gas flow in mudrocks (shales and siltstone), J. Can. Petrol. Technol. 48 (2009) 16–21.
[18] P.N. Azom, F. Javadpour, Dual-continuum modeling of shale and tight gas reservoirs, in: SPE Annual Technical Conference and Exhibition, San Antonio, Texas, USA, 2012. doi: 10.2118/159584-MS.
[19] H. Darabi, A. Ettehad, F. Javadpour, K. Sepehrnoori, Gas flow in ultra-tight shale strata, J. Fluid Mech. 710 (2012) 641–658.
[20] M. Rahmanian, R. Aguilera, A. Kantzas, A new unified diffusion–viscous-flow model based on pore-level studies of tight gas formations, SPE J. 18 (2013) 38–49.
[21] H. Singh, F. Javadpour, A. Ettehadtavakkol, H. Darabi, Nonempirical apparent permeability of shale, SPE Reservoir Eval. Eng. 17 (03) (2014) 414–424.
[22] K. Wu, X. Li, C. Guo, Z. Chen, Adsorbed gas surface diffusion and bulk gas transport in nanopores of shale reservoirs with real gas effect-adsorption-mechanical coupling, in: SPE Reservoir Simulation Symposium, Houston, Texas, USA, 2015. doi: 10.2118/173201-MS.
[23] K. Wu, X. Li, C. Wang, W. Yu, Z. Chen, A model for gas transport in micro fractures of shale and tight gas reservoirs, AIChE J. 61 (6) (2015) 2079–2088.
[24] X.C. Gao, J.C. Diniz da Costa, S.K. Bhatia, Adsorption and transport of gases in a supported microporous silica membrane, J. Membr. Sci. 460 (2014) 46–61.
[25] S.K. Bhatia, D. Nicholson, Some pitfalls in the use of the Knudsen equation in modelling diffusion in nanoporous materials, Chem. Eng. Sci. 66 (2011) 284–293.
[26] Q. Zheng, B. Yu, Y. Duan, Q. Fang, A fractal model for gas slippage factor in porous media in the slip flow regime, Chem. Eng. Sci. 87 (2013) 209–215.

[27] L. Wang, S. Liao, G. Chen, G. Guo, Z. Lu, Y. Fu, Problems and solutions for the exploration and development of shale gas reservoirs in China, Nat. Gas. Ind. 31 (2011) 119–122 (In Chinese).
[28] K.L. Milliken, M. Rudnicki, D.N. Awwiller, T. Zhang, Organic matter–hosted pore system, Marcellus formation (Devonian), Pennsylvania, AAPG Bull. 97 (2013) 177–200.
[29] X. Zhu, Q. Liao, M.D. Xin, Gas flow in microchannel of arbitrary shape in slip flow regime, Nanoscale Microscale Thermophys. Eng. 10 (2006) 41–54.
[30] M. Akbari, D. Sinton, M. Bahrami, Viscous flow in variable cross-section microchannels of arbitrary shapes, Int. J. Heat Mass Transfer 54 (2011) 3970–3978.
[31] A.W. Thornton, T. Hilder, A.J. Hill, J.M. Hill, Predicting gas diffusion regime within pores of different size, shape and composition, J. Membr. Sci. 336 (2009) 101–108.
[32] M. Bahrami, A. Tamayol, P. Taheri, Slip-flow pressure drop in microchannels of general cross section, J. Fluids Eng. 131 (2009) 031201.
[33] S.K. Prabha, P.D. Sreehari, S.P. Sathian, The effect of system boundaries on the mean free path for confined gases, AIP Adv. 3 (2013) 102107.
[34] S.K. Prabha, S.P. Sathian, Molecular-dynamics study of Poiseuille flow in a nanochannel and calculation of energy and momentum accommodation coefficients, Phys. Rev. E 85 (2012) 041201.
[35] S.K. Prabha, S.P. Sathian, Determination of accommodation coefficients of a gas mixture in a nanochannel with molecular dynamics, Microfluid. Nanofluid. 13 (2012) 883–890.
[36] F. Civan, C.S. Rai, C.H. Sondergeld, Shale-gas permeability and diffusivity inferred by improved formulation of relevant retention and transport mechanisms, Transp. Porous Media 86 (2011) 925–944.
[37] F. Javadpour, D. Fisher, M. Unsworth, Nanoscale gas flow in shale sediments, J. Can. Petrol. Technol. 46 (2007) 55–61.
[38] G. Karniadakis, A. Beskok, N. Aluru, Microflows and Nanoflows: Fundamentals and Simulation, Springer-Verlag, New York, 2005.
[39] J.G. Choi, D.D. Do, H.D. Do, Surface diffusion of adsorbed molecules in porous media: monolayer, multilayer, and capillary condensation regimes, Ind. Eng. Chem. Res. 40 (2001) 4005–4031.
[40] R.G. Loucks, R.M. Reed, S.C. Ruppel, D.M. Jarvie, Morphology, genesis, and distribution of nanometer-scale pores in siliceous mudstones of the mississippian barnett shale, J. Sediment. Res. 79 (2009) 848–861.
[41] W.V. Loebenstein, Calculations and comparisons of nonideal gas corrections for use in gas adsorption, J. Colloid Interface Sci. 36 (1971) 397–400.
[42] A. Jarrahian, E. Heidaryan, A simple correlation to estimate natural gas viscosity, J. Nat. Gas Sci. Eng. 20 (2014) 50–57.
[43] F. Civan, Effective correlation of apparent gas permeability in low-permeability porous media, Transp. Porous Media 82 (2010) 375–384.
[44] Y.S. Wei, R.J. Sadus, Equations of state for the calculation of fluid-phase equilibria, AIChE J. 46 (2000) 169–196.
[45] X.C. Gao, J.C. Diniz da Costa, S.K. Bhatia, The transport of gases in a supported mesoporous silica membrane, J. Membr. Sci. 438 (2013) 90–104.
[46] S. Loyalka, S. Hamoodi, Poiseuille flow of a rarefied gas in a cylindrical tube: solution of linearized Boltzmann equation, Phys. Fluids A 2 (1990) 2061–2065.
[47] Y. Sone, M. Hasegawa, Poiseuille and thermal transpiration flows of a rarefied gas through a rectangular pipe, J. Vac. Soc. Japan 30 (1987) 425–428.
[48] Y.H. Sun, W.K. Chan, Analytical modeling of rarefied Poiseuille flow in microchannels, J. Vac. Sci. Technol., A 22 (2004) 383–394.
[49] C. Cercignani, Theory and Applications of the Holzmann Equation, Elsevier, New York, 1975.
[50] M.M.R. Williams, Mathematical Methods in Particle Transport Theory, Butterworths, London, 1971.
[51] M.N. Kogan, Rarefied Gas Dynamics, Plenum, New York, 1969.
[52] R. Yu, X. Zhang, Y. Bian, Y. Li, M. Hao, Flow mechanism of shale gas reservoirs and influential factors of their productivity, Nat. Gas Ind. 32 (2012) 10–15 (In Chinese).
[53] M.R. Wang, Z.X. Li, Micro- and nanoscale non-ideal gas Poiseuille flows in a consistent Boltzmann algorithm model, J. Micromech. Microeng. 14 (2004) 1057–1063.
[54] S.L. Matson, J.A. Quinn, Knudsen diffusion through noncircular pores: textbook errors, AIChE J. 23 (1977) 768–770.
[55] H. Omata, L.F. Brown, Using the dusty gas diffusion equation in catalyst pores smaller than 50 Å radius, AIChE J. 18 (1972) 967–975.
[56] E.H. Kennard, Kinetic Theory of Gases with an Introduction to Statistical Mechanics, McGraw-Hill, New York, 1938.
[57] B.D. Eldridge, L.F. Brown, The effect of cross sectional pore shape on Knudsen diffusion in porous materials, AIChE J. 22 (1976) 942–944.
[58] Z. Duan, Y.S. Muzychka, Slip flow in non-circular microchannels, Microfluid. Nanofluid. 3 (2007) 473–484.
[59] G.L. Morini, M. Spiga, Slip flow in rectangular microtubes, Microscale Thermophys. Eng. 2 (1998) 273–282.
[60] G.L. Morini, M. Spiga, P. Tartarini, The rarefaction effect on the friction factor of gas flow in microchannels, Superlattices Microstruct. 35 (2004) 587–599.
[61] G.H. Tang, Y.H. Zhang, X.J. Gu, D.R. Emerson, Lattice Boltzmann modelling Knudsen layer effect in non-equilibrium flows, EPL (Europhys. Lett.) 83 (2008) 40008.
[62] M.R. Wang, Z.X. Li, An Enskog based Monte Carlo method for high Knudsen number non-ideal gas flows, Comput. Fluids 36 (2007) 1291–1297.
[63] M.R. Wang, X.D. Lan, Z.X. Li, Analyses of gas flows in micro- and nanochannels, Int. J. Heat Mass Transfer 51 (2008) 3630–3641.
[64] G.G. Michel, R.F. Sigal, F. Civan, D. Devegowda, Parametric investigation of shale gas production considering nano-scale pore size distribution, formation factor, and non-Darcy flow mechanisms, in: SPE Annual Technical Conference and Exhibition, Denver, Colorado, USA, 2011.
[65] J. Ma, J.P. Sanchez, K. Wu, G.D. Couples, Z. Jiang, A pore network model for simulating non-ideal gas flow in micro- and nano-porous materials, Fuel 116 (2014) 498–508.
[66] K. Wu, Z. Chen, H. Wang, S. Yang, X. Li, J. Shi, A model for real gas transfer in nanopores of shale gas reservoirs, EUROPEC, Madrid, Spain, 2015. doi: 10.2118/174293-MS.